Eur. Phys. J. B **52**, 37–40 (2006)
DOI: 10.1140/epjb/e2006-00275-9

THE EUROPEAN PHYSICAL JOURNAL B

Omnidirectional zero-$\bar{n}$ gap in symmetrical Fibonacci sequences composed of positive and negative refractive index materials

H.Y. Zhang[1,a], Y.P. Zhang[1], T.Y. Shang[2], Y. Zheng[2], G.J. Ren[1], P. Wang[1], and J.Q. Yao[1]

[1] College of Precision Instrument and Optoelectronics Engineering, Institute of Laser and Optoelectronics, Tianjin University, Tianjin 300072, P.R. China
[2] Henan Key Laboratory of Laser and Opto-electric Information Technology, Zhengzhou University, Zhengzhou 450052, P.R. China

Received 18 April 2006 / Received in final form 2 June 2006
Published online 6 July 2006 –

Abstract. The band structures of symmetrical Fibonacci sequences (SFS) composed of positive and negative refractive index materials are studied with a transfer matrix method. A new type of omnidirectional zero-$\bar{n}$ gaps is found in the SFS. In contrast to the Bragg gaps, such an omnidirectional zero-$\bar{n}$ gap is insensitive to the incident angles and polarization, and is invariant upon the change of the ratio of the thicknesses of two media. It is found that omnidirectional zero-$\bar{n}$ gap exists in all the SFS, and it is rather stable and independence of the structure sequence.

PACS. 41.20.Jb Electromagnetic wave propagation; radiowave propagation – 78.20.Ci Optical constants – 42.70.Qs Photonic bandgap materials

1 Introduction

Since the pioneer work of Yablonovitch [1] and John [2], photonic crystals (PCs) have been attracting a lot of attention. Photonic crystals are periodically structured dielectric media possessing photonic band gaps (PBG). The existence of band gaps prohibits the wave propagation in such media for certain frequency range. Hence a wide variety of applications have been suggested in optoelectronics and optical communications. Recent investigations of the physical properties of various groups of these deterministic media, namely, substitutional (Fibonacci, Thue-Morse, Rudin-Shapiro, and double-period) sequences have revealed that such structures exhibit certain distinctive features compared to traditional (that is, periodic and random) media. These features have become an object of great interest for scientists. Fibonacci lattice is the well-known one-dimensional (1D) quasiperiodic structure [3,4], its electronic and vibrational properties has been well-studied since the discovery of the quasi-crystalline phase in 1984 [5–7]. Light through a structure in Fibonacci sequence had also been studied in past decade [8,9], and recently the resonant states at the band edge of a photonic structure in Fibonacci sequence are studied experimentally [10].

Recently, the so-called negative refractive index materials have received renewed attention due to their novel properties such as negative refraction index, antiparallel group, and phase velocities [11–17]. Negative index materials (NIMs) which were first predicted by Veselago [11] in 1968 possess simultaneously negative permeability ε and permittivity μ. The existence of such materials with a negative refractive index was demonstrated experimentally in recent years [12,18,19] and negative index materials have become a new research topic. It has been demonstrated that the periodic stacking of alternating layers of positive and negative index material leads to a zero-$\bar{n}$ gap where the average refractive index for the stacking is close to zero. The zero-$\bar{n}$ gap is insensitive to the incident angle comparing with the ordinary Bragg gap [13,15,16].

In this paper, we study the transmission properties of symmetrical Fibonacci sequence composed of both positive and negative refractive index materials. In comparison with [9], this paper extended the previous work in [9] to general incident angles, which is one of the merits that should be emphasized.

This paper is organized as follows: the transfer matrix method for the calculation of photonic spectra and transmission coefficients is briefly introduced in Section 2; the transmission spectra for symmetrical Fibonacci sequence are calculated and discussed in Section 3, Section 4 is our conclusion.

2 Theoretical model and numerical method

A Fibonacci quasiperiodic structure is based on the Fibonacci generation scheme: $S_{j+1} = \{S_{j-1}S_j\}$ for $j \geq 1$,

[a] e-mail: zhanghuiyun1019@yahoo.com.cn

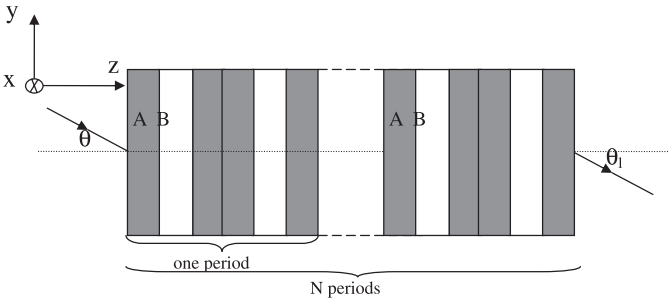

Fig. 1. Schematic representation of the SFS(3) multilayer.

with $S_0 = \{B\}$ and $S_1 = \{A\}$, the first few sequences are $S_2 = \{AB\}$, $S_3 = \{ABA\}$, $S_4 = \{ABAAB\}$ and so on. Now, let us consider a multilayer in which two types of layers A and B are arranged in a Fibonacci sequence (FS). Then, we can construct a kind of symmetric Fibonacci sequences (SFS). For the jth generation of the SFS, this symmetric sequence can be expressed as $S_{j+1} = \{G_{j+1}, H_{j+1}\}$, where G_j and H_j are FS; they obey the recursive relation, which has the form, $G_{j+1} = \{G_{j-1}G_j\}$, $H_{j+1} = \{H_jH_{j-1}\}$, $S_{j+1} = \{G_{j-1}G_j\ H_jH_{j-1}\}$. As an example, the third sequence of S_3 is $S_3 = \{ABAABA\}$. The corresponding structure of S_3 is shown in Figure 1. As can be seen from this figure, the sequence has a mirror symmetry.

In this paper, the symmetrical Fibonacci sequences (SFS) is composed of two building blocks A and B, A is the usual positive index material and B is negative index materials.

Let a wave be incident from a vacuum at an angle θ onto a SFS containing NIMs and positive index materials (PIMs), as show in Figure 1. For the transverse electric (TE) wave, the electric field **E** is assumed in the x-direction (the dielectric layers are in the $x - y$ plane), and the z-direction is normal to the interface of each layer. In general, the electric and magnetic fields at any two positions z and $z + \Delta z$ in the same layer can be related via a transfer matrix [15,16]:

$$M(\Delta z, \omega) = \begin{pmatrix} \cos[k_z \Delta z] & i\frac{\mu}{\sqrt{\varepsilon\mu - \sin^2\theta}} \sin(k_z \Delta z) \\ i\frac{\sqrt{\varepsilon\mu - \sin^2\theta}}{\mu} \sin(k_z \Delta z) & \cos[k_z \Delta z] \end{pmatrix}, \quad (1)$$

where $k_z = \omega/c\delta\sqrt{\varepsilon\mu - \sin^2\theta}$, the sign $\delta = \pm 1$. We select $\delta = 1$ for a PIMs and $\delta = -1$ for a NIMs, c is the light speed in vacuum. Then the transmission coefficient $t(\omega)$ can be obtained from the transfer matrix method [16],

$$t(\omega) = \frac{2\cos\theta}{(m_{11} + m_{22})\cos\theta + i\,(m_{12}\cos^2\theta - m_{21})}. \quad (2)$$

Here $m_{ij}(\omega)(i,\ j\ =\ 1,\ 2)$ are the matrix element of $X_N(\omega) = \prod_{j=1}^{N} M_j(d_j, \omega)$ which represents the total transfer matrix connecting the fields at the incident end and the exit end. The treatment for a TM wave is similar to that for a TE wave.

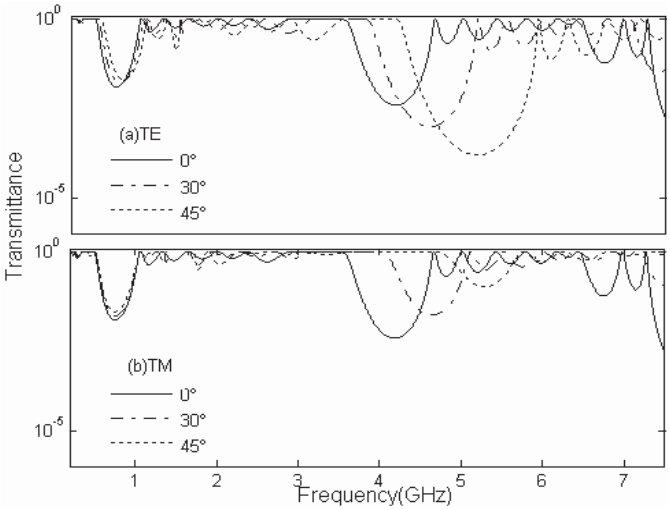

Fig. 2. Transmittance with different incident angle.

3 Results and discussion

In the following numerical investigation, we suppose a NIMs is isotropic and dispersive, with effective permeability ε and permittivity μ given by [13,20]

$$\varepsilon(\omega) = \varepsilon - \frac{\alpha}{\omega^2} \quad (3)$$

$$\mu(\omega) = \mu - \frac{\beta}{\omega^2}. \quad (4)$$

Here ω is the frequency measured in GHz, ε and μ represent permittivity and permeability of an unperturbed transmission line, α and β are circuit parameters and can be modulated with great freedom. We choose $\varepsilon = 1.21$, $\mu = 1.0$, and $\alpha = \beta = 100$. Suppose that the refractive index and thickness of a PIMs are n_1 and d_1, the refractive index and thickness of a NIMs are $n(\omega) = -\sqrt{\varepsilon(\omega)\mu(\omega)}$ and d_2, and the number of unit cells is N. Here, we use $n_1 = 2$, $d_1 = 12$ mm, $d_2 = 6$ mm, and $N = 3$.

First, we study the optical transmission spectra of SFS(3) composed of PIMs and NIMs with a mirror symmetry. The dependence of a PBG on the incident angle is shown in Figure 2. It is illustrated that the Bragg gap shifts upward in frequency for both TE and TM waves when the incident angle increases. On the contrary, the zero-$\bar{n}$ gap is insensitive to incident angle for both TE and TM polarizations. The edge of zero-$\bar{n}$ gap only shifts a little when the incident angle increases.

For comparison, the photonic band gap as a function of incident angle is plotted in Figure 3, where the white areas correspond to propagation bands and the gray areas are the forbidden bands. As shown in Figure 3, the Bragg gap shifts to high frequency for both TE and TM waves as the incident angle increases. The band edges and width of the Bragg gap are greatly affected by the polarization and the incident angle. For example, the Bragg gap of the TM wave is closed at an incident angle about 50°, whereas the zero-$\bar{n}$ gap remains nearly

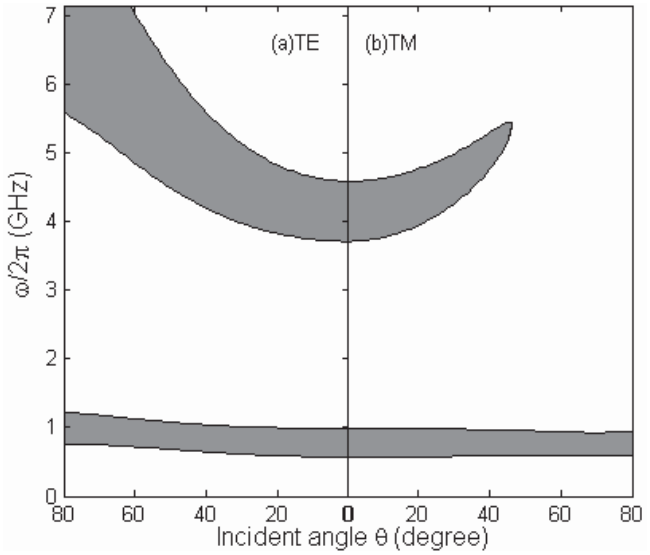

Fig. 3. The photonic band gap as a function of incident angle.

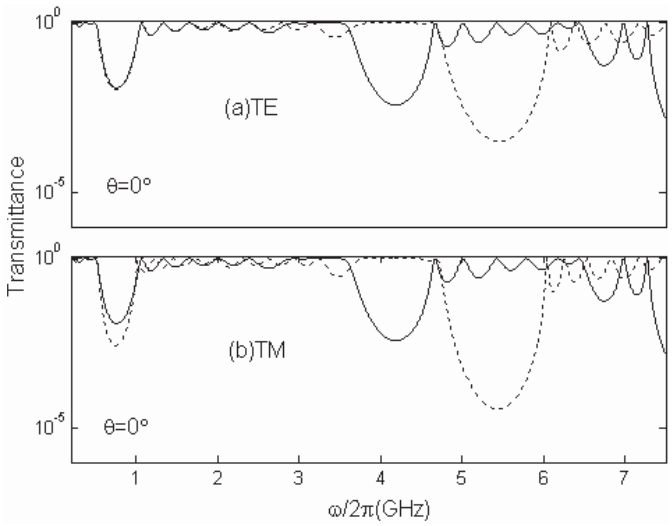

Fig. 4. Transmittance with different the ratio of the thicknesses.

invariant under a various incident angle for both TE and TM polarizations. Even when incident angle increases to 80°, the edge of zero-$\bar{n}$ gap only shifts a little. The insensitivity of the edge to the incident angle and polarization indicates that there exists an omnidirectional gap coming from the zero-$\bar{n}$ gap mechanism. The omnidirectional zero-$\bar{n}$ gap possesses some unique properties compared to the usual omnidirectional Bragg gap. These properties may provide us aspects for applications, such as omnidirectional reflector with a *fixed* bandwidth.

In Figure 4, we show the dependence of the gaps on the ratio of the thicknesses of the two media at normal incidence. The solid line is the transmittance through the structure with thickness of $d_1 = 12$ mm, $d_2 = 6$ mm. The dashed line corresponds to the transmittance through the same media but the unit cell size is scaled by 3/4. It is clear from Figure 4 that Bragg gap is affected greatly by

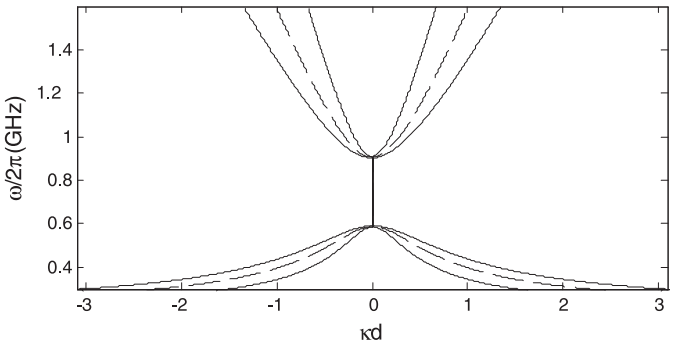

Fig. 5. The variance of band gap with different ratio of two media. Solid line: $d_1 = 12$ mm, $d_2 = 6$ mm. Dashed line: the lattice constant is scaled by 2/4. Dotted line: the lattice constant is scaled by 3/4.

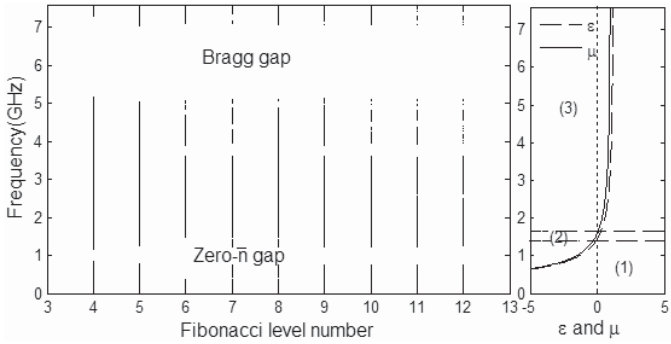

Fig. 6. The left panel: the photonic spectra for the first nine successive levels of Fibonacci photonic structures; the right panel: numerical values of $\varepsilon(\omega)$ and $\mu(\omega)$ given by equation (3).

the change of the ratio of the thicknesses. Conversely, the zero-$\bar{n}$ gap remains invariant with the ratio of the thicknesses.

In order to understand the dependence of the gaps on the ratio of the thicknesses of the two media, we interpret the behaviors using the dispersion relation. For the SFS(3), the dispersion relation is [21]:

$$\cos\kappa(\boldsymbol{d}_1+\boldsymbol{d}_2) = \cos(2\boldsymbol{k}_1\boldsymbol{d}_1)\cos(\boldsymbol{k}_2\boldsymbol{d}_2) - \frac{1}{2}\left(\frac{\eta_1}{\eta_2}+\frac{\eta_2}{\eta_1}\right)\sin(2\boldsymbol{k}_1\boldsymbol{d}_1)\sin(\boldsymbol{k}_2\boldsymbol{d}_2), \quad (5)$$

where $\kappa(\boldsymbol{d}_1+\boldsymbol{d}_2)$ is the Bloch phase, the wave impedances and effective phase shifts in PIMs and NIMs layers are $\eta_i = \sqrt{|\mu_i/\varepsilon_i|}$, $\boldsymbol{k}_i\boldsymbol{d}_i = \boldsymbol{k}\sqrt{|\varepsilon_i\mu_i|}\boldsymbol{d}_i$ $(i = 1, 2)$, respectively; $\boldsymbol{k}$ is the wave number in vacuum. The variance of band gap with different ratio of two media is shown in Figure 5. It is shown that the zero-$\bar{n}$ gap (0.6–0.9 GHz) hardly changes with the ratio of the thicknesses. But the Bragg gap will shift noticeably while the width of the gap will change a little when the ratio of the thicknesses of the two types of layers varies.

Now, we turn to study the photonic spectra for the other successive FS of the quasiperiodic structure, i.e., for S_4 to S_{12}. The photonic spectra is schematically shown in the left panel of Figure 6, the right panel shows numerical

values of $\varepsilon(\omega)$ and $\mu(\omega)$ given by equation (3), here the three frequency ranges from low to high: (1) $\varepsilon < 0$, $\mu < 0$, (2) $\varepsilon > 0$, $\mu < 0$, (3) $\varepsilon > 0$, $\mu > 0$. It is illustrated that for each FS there always open two broad gaps in the considered frequency range beside some minor gaps in other frequency range. The broad gap at low frequency (gap1, hereafter) lies in range 1, where $\varepsilon < 0$, $\mu < 0$, while that at high frequency (gap 2) lies in range 3, where $\varepsilon > 0$, $\mu > 0$. It has known that the gap1 is a zero-$\bar{n}$ gap while gap 2 is a Bragg gap [13,15–17]. From the spectra for S_4 to S_{12}, we note that zero-$\bar{n}$ gap vary with the sequence number at first few levels, but beginning from S_8, the gap begin to become stabilized, with fixed gap positions and size. The positions and size of the Bragg gap hardly change, while the frequency about Bragg gap is split more and more.

4 Conclusion

To conclude, using the transfer matrix method, we have discussed the photonic spectra of SFS containing positive and negative refractive index materials. We have shown that a new type of omnidirectional gaps is found in the SFS. In contrast to the Bragg gaps, such an omnidirectional gap is insensitive to the incident angles and polarization, and is invariant upon the change of the ratio of the thicknesses of two media. It is found that zero-$\bar{n}$ gap exists in all the SFS, and it is rather stable and independence of the structure sequence.

This work was supported by the National High Technology Research and Development Program of China under Grant No. 2002AA311190, and by the Optoelectronic Unite Science Research Center of Tianjin (No. 013184011).

References

1. E. Yablonovitch, Phys. Rev. Lett. **58**, 2059 (1987)
2. S. John, Phys. Rev. Lett. **58**, 2486 (1987)
3. C.J. Jin, B.Y. Cheng, B.Y. Man, Z.L. Li, D.Z. Zhang, Phys. Rev. B **61**, 10762 (2000)
4. M.E. Zoorob, M.D.B. Charlton, G.J. Parker, J.J. Baumberg, M.C. Netti, Nature **404**, 740 (2000)
5. W. Gellermann, M. Kohmoto, B. Sutherland, P.C. Taylor, Phys. Rev. Lett. **72**, 633 (1994)
6. J.P. Lu, T. Odagaki, J.L. Birman, Phys. Rev. B **33**, 4809 (1986)
7. V. Kumar, G. Ananthakrishna, Phys. Rev. Lett. **59**, 1476 (1987)
8. J. Li, D. Zhao, Z. Liu, Phys. Lett. A **332**, 461 (2004)
9. H. He, W.Y. Zhang, Phys. Lett. A **351**, 198 (2006)
10. L. Dal Negro, C.J. Oton, Z. Gaburro, L. Pavesi, P. Johnson, A. Lagendijk, R. Righini, M. Colocci, D.S. Wiersma, Phys. Rev. Lett. **90**, 055501 (2003)
11. V.G. Veselago, Sov. Phys. Usp. **10**, 509 (1968)
12. D.R. Smith, W.J. Padilla, D.C. Vier, S.C. Nemat-Nasser, S. Schultz, Phys. Rev. Lett. **84**, 4184 (2000)
13. J. Li, L. Zhou, C.T. Chan, P. Sheng, Phys. Rev. Lett. **90**, 083901 (2003)
14. A.A. Houck, J.B. Brock, I.L. Chuang, Phys. Rev. Lett. **90**, 137401 (2003)
15. L.G. Wang, H. Chen, S.Y. Zhu, Phys. Rev. B **61**, 10762 (2000)
16. H.T. Jiang, H. Chen, H.Q. Li, Y.W. Zhang, S.Y. Zhu, Appl. Phys. Lett. **83**, 5386 (2003)
17. H.T. Jiang, H. Chen, H.Q. Li, Y.W. Zhang, J. Zi, S.Y. Zhu, Phys. Rev. E **69**, 066607 (2004)
18. R.A. Shelby, D.R. Smith, S.C. Nemat-Nasser, S. Schultz, Appl. Phys. Lett. **78**, 489 (2001)
19. R.A. Shelby, D.R. Smith, S. Schultz, Science **292**, 77 (2001)
20. J. Pacheco Jr., T.M. Grzegorczyk, B.I. Wu, Y. Zhang, J.A. Kong, Phys. Rev. Lett. **89**, 257401 (2002)
21. D. Lusk, I. Abdulhalim, F. Placido, Opt. Commun. **198**, 273 (2001)